Nat. Hazards Earth Syst. Sci. Discuss., 1, 3689–3734, 2013
www.nat-hazards-earth-syst-sci-discuss.net/1/3689/2013/
doi:10.5194/nhessd-1-3689-2013

Natural Hazards and Earth System Sciences
Discussions

Analysis of sea cliff slope stability integrating traditional geomechanical surveys and remote sensing

S. Martino[1,2] **and P. Mazzanti**[1,2]

[1]Department of Earth Sciences, University of Rome "Sapienza", P.le Aldo Moro n.5, 00185, Rome, Italy
[2]CERI Research Center, University of Rome "Sapienza", P.le U. Pilozzi n.9, 00038, Valmontone, Italy

Received: 28 June 2013 – Accepted: 13 July 2013 – Published: 31 July 2013

Correspondence to: P. Mazzanti (paolo.mazzanti@uniroma1.it)

Published by Copernicus Publications on behalf of the European Geosciences Union.

Abstract

An integrated approach to the geomechanical characterization of coastal sea cliffs was demonstrated at Mt. Pucci (Gargano promontory, Southern Italy) by performing d[et] traditional geomechanical and remote geostructural investigations via Terrestrial Laser Scanner (TLS). The consistency of the integrated techniques allowed us to achieve a comprehensive and affordable characterization of the main joint sets on the sea cliff slope. The observed joint sets were observed to evaluate the susceptibility of the slope to rock falls by attributing safety factors (SFs) to the topple- and wedge-prone rock blocks under three triggering conditions: (a) filling with static water, (b) seismic action, and (c) weathering of joint surfaces. The results of the susceptibility analysis for the topple-prone blocks show that the critical height of water filling of the joint is up to 50 cm and that the critical pseudo-static acceleration values vary in the range of 0.16–0.3 g depending on the block geometry and slope face orientation. For the wedge blocks, the critical height of water filling of the joint is generally up to several centimeters, and the critical pseudo-static acceleration values vary in the range of 0.05–0.8 g depending on the block geometry and slope face orientation. Moreover, the unstable conditions of the blocks due to weathering generally represent 60 % of the joint degradation of the intact rock. The combined action of weathering and static water fill was also considered, resulting in a significant decrease of the SFs. Specifically, unstable conditions are associated with water levels lower than 47 % of the water levels observed in intact joints, even if less than 60 % of the weathering is attributed to the joints. Furthermore, remote survey analyses via Thermal InfraRed Camera and Terrestrial SAR Interferometry (TInSAR) were performed to evaluate the role of the surveyed joint sets in inducing instabilities in the Mt. Pucci sea cliff. The results of this study can be summarized as follows: (i) the thermal images allowed us to identify anomalies that correspond well to the main joints and to the slope material released due to recent collapses; and (ii) TInSAR monitoring revealed permanent displacements greater than 1 mm and cyclic daily

displacements of up to 1.2 mm were detected in certain sectors and were attributed to thermal variation of the rock mass.

1 Introduction

Due to the rapid development of coastal settlements and the increasing population located in coastal regions, substantial efforts are required to manage the possible risks associated with natural hazards in these areas. It is estimated that greater than 37 % of the world's population live within 100 km of the coastline and that 80 % of these shores are rocky (Emery and Kuhn, 1982). Landslides are one of the main threats in this environment because they entail the additional risk of tsunamis, as demonstrated by several recent events (e.g., Assier-Rzadkiewicz et al., 2000; Tappin et al., 2001; Papadopoulos and Kortekaas, 2003; Tinti et al., 2004; Mazzanti and Bozzano, 2011).

In addition to coastal settlements, rapid landslides can be particularly dangerous for near-shore structures and infrastructure, such as oil platforms and submarine pipelines. These structures can be severely damaged by coastal landslides in both the detachment areas and the regions affected during propagation (e.g., Heezen and Ewing, 1952; Assier-Rzadkiewicz et al., 2000; Bozzano et al., 2011; L'Heureux et al., 2011).

Although they are not the most dangerous events, rock falls, topples, and large collapses from sea cliffs are the most common slope instabilities in coastal regions. These events commonly involve small volumes (e.g., single blocks), but they may involve larger sizes, thus significantly increasing the risk to near-shore settlements and activities (Hampton et al., 2004).

Furthermore, rock falls are a fundamental component of landscape evolution in rocky coasts, contributing to a high erosion rate, which can reach several decimeters per year (Duperret, 2002, 2004; Mortimore, 2004).

Rock falls are a widespread problem on high coastal cliffs, and in certain regions, these cliffs represent a large percentage of the total coast. For example, 15 % of the

Italian coasts are rock cliffs. Furthermore, the prediction of coastal rock falls is quite complex, and physical investigation is the most common approach for hazard assessment purposes.

This paper reports the results of a detailed investigation carried out on a 45 m-high sea cliff for the assessment of its overall stability by examining different triggering processes. The sea cliff, located in the Gargano National Reserve (Southern Italy), is composed of fractured and weathered limestones and chalks and is frequently affected by rock falls. In this study, data collected from traditional field surveys were integrated with (i) pervasive joint set characterization using a Terrestrial Laser Scanner (TLS)-derived high-resolution point cloud and (ii) identification of micro-movements of the localized blocks via three days of continuous Terrestrial SAR Interferometry (TInSAR) (Mazzanti, 2011) monitoring. Furthermore, a preliminary assessment of the rock mass thermal features was carried out based on multi-temporal Terrestrial Infra-Red Thermography (TIR) surveys.

The aim of this study is to provide technical guidelines for designing a monitoring system devoted to providing alerts for rock fall events by integrating different devices able to detect external actions, failure precursors, and strain effects.

2 Sea cliff investigation and landslide hazards

Among coastal slopes, high cliffs are of particular interest in terms of risk mitigation because of their complex evolution that involves the coupled action of marine erosion and gravity-induced slope instability (Hampton et al., 2004).

The high rate of occurrence of slope failures affecting costal cliffs is hazardous not only because of the direct effect of the falling masses but also as a result of induced effects, such as tsunamis (resulting from falls that land in the sea), shock wave propagation (resulting from falls that land on the shore), and the development of new fractures along the cliff edge.

To reduce the risk associated with these phenomena, advanced and multi-parameter techniques are now available for monitoring cliffs subject to erosion and sudden collapse. This approach requires the integration of geophysical and geological investigations to foresee the slope failure and to provide civil protection agencies with an effective tool to alert and secure people and structures exposed to the event.

Because of the morphology and height of coastal cliffs, non-conventional investigation techniques must be applied to the cliff wall. Similarly, the installation of remote monitoring devices (e.g., TLS, TInSAR, TIR) requires specialized technical implementation because the visibility of the cliff wall from the ground is often limited.

Field mapping of rock discontinuities is the most common approach for analysis of rock cliffs. This classical geomechanical investigation allows the main joints to be characterized in terms of dip, dip direction, widening, the presence of gouge material, persistency, and other factors (see Hatheway, 2009 for a comprehensive review). Furthermore, the mechanical features of the rock mass, including the surface roughness and the rock compressive strength, can be assessed with field instruments and laboratory experiments. High coastal cliffs are difficult access directly and, therefore, cannot be easily investigated using traditional field methods (Cheryl and Hapke, 2004), resulting in high costs or, more often, low information density.

The monitoring of cliff slopes must be specifically adapted to the different evolutionary stages that characterize individual coastal slopes and must consider both the level of risk and spatial distribution of these slopes. Cliff slope evolution is strongly conditioned by the geological setting and by the jointing conditions of the involved rock masses. Surveying these features and inventorying the slope instabilities enables the performance of statistically based analyses of the susceptibility of sea cliffs to rock falls (Lee et al., 2001, 2002; Lim et al., 2010; Marques et al., 2011). In addition to the most common preconditioning and triggering factors that control rock falls from inland cliffs (e.g., rainfall, earthquakes, cyclic temperature variations, plant root growth), further factors must be considered for coastal cliffs. For example, tidal variations, basal

erosion induced by waves, and sea storms induce additional stresses on the rock mass (Senfaute et al., 2009; Violante, 2009 and references therein).

A basic conceptual model of the evolution of a sea cliff toward a coastal slope can be summarized in the three following steps (Fig. 1):

1. “Persistent sea cliff”: a sea cliff evolves via progressive retreat as an effect of shoreline erosion due to sea waves. In this stage, the slope instabilities are primarily represented by rock falls and toppling, i.e., gravitational instabilities characterized by impulsive and recurrent events.
2. “Seasonal sea cliff”: the sea cliff is affected seasonally by marine erosion only as an effect of the strongest sea storms, and a talus deposit is formed during the non-storm periods.
3. “Coastal slope”: the sea cliff is definitively abandoned by the sea, no marine erosion occurs except during exceptional storm events, a beach is formed that separates the old cliff from the present shoreline, and the slope retreat of the coastal slope is primarily due to sliding mechanisms, which cause a progressive decrease in the slope angle.

The model of the sea cliff evolution described above corresponds to a gradual reduction in the natural risks of the coastal area (Marques, 2008, and references therein).

With reference to the above-listed stages, it is possible to associate the “persistent cliff slope stage” with a natural risk consisting of impulsive rock fall events that can produce tsunami waves, which affect the adjacent pocket beaches. In addition, the instantaneous retreat of the cliff can drastically affect structures or buildings located along the sea cliff border.

In the “seasonal cliff slope stage,” the natural risk is related to impulsive events that can affect an emerged beach, i.e., during the non-storm period, constituting a potential hazard for visitors.

Finally, the “coastal slope stage” corresponds to a minor risk for visitors because the landslide mechanisms are different. Typical preconditioning and triggering factors

related to the sea action are no longer effective; hence, the instabilities are less abrupt. However, in this stage, larger landslides may occur, leading to major risks for structures or infrastructure located near the top of the cliff slope.

3 Geological and geomorphological setting of the Mt. Pucci sea cliff

The Gargano promontory is a portion of the carbonatic Apulia Platform that represents one of the most important paleogeographic units of the middle-southern Italian Apennine (Bosellini et al., 1999). This paleogeographic unit was formed during the Mesozoic (from the lower Jurassic up to the middle Cretaceous period) in Bahamas-like conditions, and it currently represents the most external domain of the Apennine Chain in the southern Adriatic area. According to Bosellini and Morsilli (1997), beginning in the middle-upper Cretaceous and throughout the Paleocene, the Apulia Platform was gradually destroyed due to the combined effects of eustatism (also responsible for many Paleocene emersion phases), tectonic uplift, and strong earthquakes. This destruction is evidenced by megabreccia deposits (Grottone deposits) and bioclastic turbidites (Peschici Formation), which widely outcrop in the Gargano area (Bosellini and Morsilli, 1997).

The Gargano promontory area is characterized by EW-oriented tectonic elements corresponding to transform fault lines (Billi and Salvini, 2000), and in particular, it constitutes a horst involved in a wide anticline fold system with a WNW–ESE-oriented axis. This anticline structure is crossed by numerous faults that have left transtensive mechanisms with orientations varying from E–W to NW–SE. These faults are primarily concentrated in the southern portion of the area, corresponding to the anticline hinge. Among these elements, the Mattinata fault represents the main regional structure related to an evident local geomorphological landform (Billi and Salvini, 2000) and to many seismogenetic sources capable of earthquakes up to M_w = 6.4 (DISS3.1, 2010) that are expected with a return time from several hundred to several thousand years.

Based on the CEDIT catalogue (Fortunato et al., 2012), any earthquake-induced effects were historically documented on the northern coast of the Gargano promontory.

The Mt. Pucci sea cliff is located on the northern side of the Gargano promontory, close to the village of Peschici. Mt. Pucci exhibits a hill-type relief with a maximum elevation of approximately 150 m a.s.l. (Fig. 2). According to the wavemeter records, the most frequent sea storms in the Gargano promontory originate from the NE, and the height of the strongest waves reaches 4 m, with a frequency of 10–25 %. Notably strong storms are only rarely recorded from the N, with a maximum wave height of 5.2 m (ISPRA, 2012).

According to Bosellini and Morsilli (2001) and based on surveys filed by the same Authors, the following geological formations outcrop in the study area:

- Maiolica (MA) Formation (lower Cretaceous): micritic white limestone with chert, mildly to thinly layered;
- Scisti a Fucoidi (SF) Formation (lower Cretaceous): white micritic limestone and gray marly limestone, mildly to thinly layered;
- Scaglia (SC) Formation (lower–middle Cretaceous): white marly limestone with brown chert, mildly to thinly layered;
- Peschici (PSH) Formation (Eocene): white bioclastic calcarenite with nummulites and echinids, mildly to thickly layered.

In particular, the PSH and the SC Formations outcrop on the Mt. Pucci sea cliff with a 30/10 (dip direction/dip) attitude in the strata.

Field evidence reveals that the Mt. Pucci coastal cliff is widely involved in rockslides responsible for a clearly visible talus at the bottom of the slope (Fig. 3). The main predisposing conditions for these instabilities are the subvertical face of the cliff and the intense erosion processes due to the sea, which continuously excavates the base of the cliff. Moreover, the visible weathering processes can be primarily related to intense

thermal variation (both diurnal and seasonal) due to the north-facing aspect of the cliff as well as to the nebulized salt water from the sea waves.

The annual average rainfall measured at Vico del Gargano (close to Peschici) is 810 mm yr^{-1}, with an average annual temperature of approximately 15 °C (Polemio et al., 2000).

4 Geomechanical investigation of the Mt. Pucci sea cliff

Based on the previously reported model of the evolution of a cliff slope toward a coastal slope (cf. Sect. 2), Mt. Pucci represents a persistent sea cliff, corresponding to the first stage of the above-depicted evolution model. The geomechanical investigations in this study were focused on the reconstruction of the rock mass joint setting because it represents a fundamental feature that defines the failure model for the sea cliff during the initial stage, and on the evaluation of landslide susceptibility and the stability conditions of the slope.

Direct traditional geomechanical field surveys and remote laser scanner surveys were performed. These investigations aimed to verify the reliability and efficacy of true-color 3-D accurate point clouds for measuring the attitude of the main joints of rock masses in inaccessible areas. Furthermore, the investigations aimed to understand how the combination of traditional and laser scanner surveys can be integrated to provide more accurate and complete information.

4.1 Direct geomechanical survey

The geomechanical characterization of the calcarenites and the marly limestones that outcrop on the Mt. Pucci coastal cliff slope (ascribable to the PSH and SC Formations, respectively) was carried out via a traditional geomechanical survey performed according to the ISRM (2007) standard. This survey was focused on evaluating and dimensioning both the rock mass jointing conditions and the strength properties and

aimed to identify the main joint sets of the rock masses together with their attitude, geomechanical properties (i.e., spacing, opening, jointing conditions, standard joint indexes Jv and Ib – ISRM, 1978, 2007), and strength parameter values (using a Schmidt Hammer sclerometer and a Barton Comb. profilometer).

Due to the reduced accessibility of the cliff slope, 11 geomechanical scanlines were performed on the surrounding cliff area (Fig. 2), including nine on the PSH calcarenites and two on the SC marly limestones. Four other geomechanical scanlines were directly carried out by climbers on the wall of the coastal cliff slope where the PSH calcarenites outcrop.

The poles of the measured joints were plotted using the code "*RockScience Dips – free demo version*" from the Schmidt equi-areal stereographic projection (lower hemisphere). The attitudes of the main joint sets were deduced, as suggested by ISRM (1978), using Fisher concentration contour lines and attributing a joint set attitude if the concentration value was greater than 5 %. Following this approach, five main joint sets (J1 to J5) were recognized in the PSH calcarenites, and only two main joint sets were recognized in the SC marly limestones (see Table 1 for the joint set parameters). For both the PSH and the SC rock masses, the J1 set corresponds to stratification.

The strength parameter values of the joint sets were attributed according to the Barton and Bandis (1973, 1990) failure criterion:

$$\tau_p = \sigma_n \tan(\varphi_b + \mathrm{JRC}\log(\mathrm{JCS}/\sigma_n)) \quad (1)$$

where τ_p is the shear strength of the joint, σ_n is the normal stress acting on the joint surface, φ_b is the intact rock friction angle, JRC is the Joint Roughness Coefficient attributed by the Barton profilometer, and JCS is the Joint Compressive Strength measured by the Schmidt sclerometer.

The φ_b values were obtained from datasets in the literature using the UCS strength values derived from point load tests and laboratory measurements specifically performed on both the PSH calcarenites and the SC marly limestone (Table 2) according to the ASTM D5731-08 (2008) and ISRM (1977, 1985) standards.

4.2 Remote measurements: laser scanner surveys

Remote geomechanical surveys were performed using a laser scanner integrated with a high-resolution digital camera and supported by a D-GPS survey.

Surveys were performed on 12 November 2010, using a Riegl VZ400 Laser Scanner combined with a Nikon D700 camera with a 14 mm lens and a luminosity of 1.2 and one GPS-Glonass unit (model Topcon Hyper Pro).

Data were collected from two different positions to reduce the shadow zones and to obtain mm-scale accuracy of the detected points (Fig. 4). Nevertheless, due to the difficult accessibility of the cliff and the unfavorable exposition of the cliff face, it was not possible to achieve a "shadow free" point cloud. Optical markers were applied all around the monitored area to align the data collected from the two positions and to translate the detected coordinates to the UTM-WGS84 coordinate system via the built-in GPS sensor (Fig. 4). Furthermore, the RGB colors of the detected points were collected using the Nikon D700 digital camera integrated with the VZ400 sensor. Hence, a true-color point cloud of the cliff consisting of approximately 45M points with a point density of approximately 1 point cm^{-1} was achieved (Fig. 5).

Both manual and automatic analyses of the point cloud were performed to derive information on the joint pattern and its features. Specifically, the AdHoc3-D software (http://www.adhoc3d.com/en/adhoc/) was used for manual analysis, which was performed by two researchers to reduce the subjectivity in the identification of joints. Automatic analysis was performed using both the Split-FX-Free Demo Version (http://www.spliteng.com/split-fx/) and the Coltop3-D-Free Demo version (Jaboyedoff et al., 2007) software (Fig. 6).

Using the Split-FX software, the automatic analysis identified a sufficient number of points (whose number can be defined by the operator) depicting a surface whose orientation in space can be measured. Such an approach allowed us to perform detailed analyses of the entire outcropping cliff (by analyzing a large amount of surfaces in few minutes) and represents an objective analysis, i.e., one that is not influenced by the

operator. Furthermore, the high-density point cloud joint information can be derived at different scales (including small surfaces).

However, certain weaknesses of performing an "automatic analysis" must be accounted for. First, not all exposed surfaces can be identified, such as the limestone stratification that is parallel to both of the TLS points of view in the case of Mt. Pucci (Fig. 4). Second, the sizes of the exposed surfaces used for the automatic recognition are crucial, and their selection requires a skilled evaluation by the operator. Moreover, the Mt. Pucci data were collected only on the eastern side of the cliff (Fig. 4), and hence, the rock joints with an approximately westerly dip direction cannot be identified.

However, "manual analysis" allowed us to avoid certain limitations that affect the "automatic analysis," enabling us to characterize the stratification joint set in detail.

Table 3 summarizes the main joint sets and their average spacing values derived from the remote measurements for the PSH and the SC formations. Two main joint sets were identified in the SC Fm., and four main joint sets were detected in the PSH Fm.

A comparison between Tables 1 and 3 shows that the joint set data derived from traditional field surveys and from traditional geomechanical scanlines are quite similar, except for the secondary joint set J2 for the SC Fm. This difference may be related to the distance between the unique available geomechanical station on the SC Fm. and the Mt. Pucci sea cliffs; specifically, local structural control might be the cause of such a difference (see Fig. 2). These results confirm the reliability of the simplified geomechanical analysis derived from the TLS data.

All of the available data, from both manual and TLS surveys, were used for computation of the Jv parameter (Palmstrom, 1982, 1985, 1986, 1996; Sen and Eissa, 1992). Jv values of 3.2 and 9.7 were estimated for the PSH Fm. and the SC Fm., respectively (Table 3).

Figure 7 displays the final stereo-plots derived from the combined automatic and manual analysis of the TLS point cloud for the PSH Fm. and SC Fm., respectively and

Table 4 summarizes the geomechanical parameters attributed to all the distinguished joint sets.

5 Susceptibility to rock falls and topples

The stability conditions of the Mt. Pucci sea cliff were analyzed by taking into account the jointing conditions of the rock mass that outcrops on the slope face.

The evolution of a sea cliff toward a costal slope predisposes it to different landslide mechanisms related to weathering and jointing conditions, which gradually change with the evolving slope instabilities (see the evolutionary model sketched in Fig. 1). However, in the "persistent sea cliff stage", the cliff retreat is characterized by stiff outcropping rocks characterized by high-angle primary joint sets. The progressive retreat and the resulting stress release cause the generation of secondary joint sets that are nearly parallel to the slope face and whose openings generally increase with decreasing distance from the cliff; these joints favor failures of the slope face, such as falls and topples.

In the "seasonal sea cliff stage", the average rate of retreat decreases, and the longer exposition of the cliff causes the weathering processes to occur more intensively, predisposing the cliff to more intense instabilities during storm periods.

Finally, in the "coastal slope stage", the secondary joint sets are not necessarily located parallel to the slope face, and intense weathering processes can occur that favor landslide triggers and control the strain rate of the sliding processes.

The primary (i.e., strata) and secondary (i.e., fractures) joint sets in the Mt. Pucci sea cliff play a fundamental role in controlling the slope instabilities.

Three failure mechanisms were therefore considered for the slope stability analysis (Duncan and Christopher, 2004) by considering the attitude of the main measured joint sets: (1) rock plane sliding, (2) rock topples, and (3) rock wedge slides.

For each considered failure mechanism, a preliminary kinematic analysis was performed using the Markland (1972) tests for both slides and topples. The tests were

performed by considering all of the possible combinations of joint sets and identifying those capable of meeting the established kinematic criteria. Moreover, to perform a more detailed kinematic analysis, four slope face orientations (dip direction/dip) were considered (355/80, 320/75, 345/70, and 300/60, as measured from east to west along the cliff wall), based on the point cloud provided by the laser scanner survey in addition to the average orientation of the sea cliff slopes (330/70).

A stability analysis was performed for these combinations of joint sets to attribute an SF under different destabilizing conditions. For rock wedge sliding, the kinematic test was performed simultaneously with the slope stability analysis using the code "*Wedge Failure Analysis Version 2.0- free version*".

The Markland tests provided the following outputs:

1. as it is reported in Table 5, kinematic compatibility with rock topples exists only in the case of the 355/80-oriented slope face by combining the sub-horizontal stratification set J1 with the sub-vertical joint set J3 of Table 4 and by considering all combinations with the other sets (J2, J4, J5) as lateral joints;

2. kinematic compatibility with rock wedge sliding exists for all of the slope face orientations except for the PSH calcarenites alone and the combinations of joint sets reported in Table 6;

3. no kinematic compatibility exists with rock plane failures.

6 Stability conditions of the Mt. Pucci sea cliff

The stability conditions of the Mt. Pucci sea cliff were tested for rock topples and rock wedge sliding because these two mechanisms showed kinematic compatibility based on the Markland tests.

The stability analyses were performed under static and pseudo-static conditions (i.e., considering seismic action). In addition, possible destabilizing factors were taken into

account, such as static water pressure within the joint sets and weathering of the joints (the latter was applied to the rock wedge sliding mechanism only).

In the case of rock topples, considering the joint properties summarized in Table 4, the stability chart of Fig. 8 (Goodman and Bray, 1977) demonstrates that stable conditions can be expected for the coastal cliff wall of Mt. Pucci under static conditions and without external actions. Based on these equilibrium conditions, the static level of the water filling the subvertical set J3 should reach approximately 50 cm before causing block toppling.

Moreover, if a pseudo-static acceleration k_x is applied to the blocks, i.e., the weight force is deflected downslope, the critical pseudo-static acceleration k_y required to reach disequilibrium condition and cause block toppling is expressed by the following equation:

$$\tan\Delta_\alpha = (\tan\beta - \tan\psi) = k_y \quad (2)$$

where Δ_α = deflection angle, $\beta = (b/h)$ = geometrical ratio of the block (where b is the length and h is the height of the block), and ψ = dip angle of the basal plane.

According to Eq. (2), the average critical pseudo-static acceleration (k_y) for triggering rock topples is equal to 0.25 g, which corresponds to a return time of approximately 1000 yr for the Mt. Pucci area (INGV, 2006).

In the case of rock wedge sliding, the stability analysis was performed using the code "*Wedge Failure Analysis Version 2.0 – free version*" and adopting the approach of Hoek and Bray (1981). The wedge geometries were hypothesized by combining the five individuated joint sets and assuming the presence of tension cracks (if the intent was to adapt this role with respect to the slope face orientation). This condition results in the 335/80 slope face orientation when considering the 358/90 joint set.

Because no rock wedges resulted for the SC marly limestones, the stability analysis was performed only for the PSH calcarenites. The results from the data reported in Table 5 show that stable conditions were found for all of the hypothesized joint set combinations under static conditions.

Nevertheless, three possible destabilizing conditions were taken into account: (a) static water filling of the joints, (b) seismic action, and (c) weathering of the joint surface.

The static action due to (a) water filling of the joints was taken into account by assuming distributions of isotropic stresses all around the block; such distributions were integrated along the joint surfaces to compute the incremental lateral forces exerted by the water. By increasing the water level within the joint, the critical conditions for the block equilibrium were determined, indicating a critical value of the water-height (Zw_{cr}) that must be assumed for each wedge geometry, as summarized in Table 6. From the results of this analysis, a few tenths of a centimeter of water filling can be responsible for causing disequilibrium conditions.

The seismic action (b) was considered by assuming a pseudo-static horizontal acceleration and computing the safety factor SF according to the simplified equations of Hoek and Bray (1981):

$$SF = [(R_A + R_B)\tan\varphi_{av}]/W\,\mathrm{sen}\psi_i \quad (3)$$

$$(R_A + R_B) = [(W\cos\psi_i - W\,k_x\,\mathrm{sen}\psi_i)\,\mathrm{sen}\beta]/[(W\,\mathrm{sen}\psi_i + W\,k_x\cos\psi_i)\,\mathrm{sen}(\xi/2)] \quad (4)$$

where W = weight force; R_A and R_B = resistance forces acting normally to the wedge planes A and B, respectively; φ_{av} = fiction angle of the wedge joints (in this simplified equation, the value is the same for the two joints and is assumed equal to an average friction value); ψ_i = angle of inclination of the intersection line between the two wedge planes measured with respect to the horizontal line; ξ = wedge opening angle (measured between the dip directions of the planes A and B); and k_x = pseudo-static horizontal coefficient.

According to Eqs. (3) and (4), the critical pseudo-static acceleration k_y was derived for each block geometry. Moreover, the SFs were computed for the local pseudo-static horizontal acceleration corresponding to return times of 475 yr and 2475 yr, i.e., equal to 0.169 g and 0.316 g, respectively (INGV, 2006). The results of the data reported in Table 6 show that many wedge geometries remain stable for the maximum expected seismic action.

With respect to (c) the weathering of the joints, a theoretical reduction of the strength values was assumed depending on the weathered friction angle φ_{wth} and computed with the following empirical equation (De Vallejo, 2005):

$$\varphi_{wth} = (\varphi_b - 20°) + 20\,(r/R) \quad (5)$$

where R = Schmidt sclerometer rebound value obtained for an intact joint, r = Schmidt sclerometer rebound value obtained for a weathered joint, and φ_b = internal fiction angle of the intact rock.

The $SF_{r/R}$ values computed under weathered conditions (i.e., by assuming different values of the r/R weathering ratio) demonstrate that unstable conditions for the blocks are generally reached for greater than 60 % weathering of the joints (Table 6), corresponding to a highly significant reduction of the strength values with respect to the intact joint.

However, if a combined action due to weathering and static water filling of the joints is assumed, the computed SF values exhibit a different behavior: when less than 60 % weathering is attributed to the joints, unstable conditions are generally reached for water levels lower than 47 % with respect to those required to cause unstable conditions in the case of intact joints.

7 Cliff slope monitoring

7.1 Preliminary monitoring activities

The Mt. Pucci cliff was also used as a test site for evaluating the effectiveness of Terrestrial Remote Sensing in providing useful information on the cliff stability conditions. Over the last few decades, several ground-based remote sensing techniques have been developed (Mazzanti, 2012). These techniques use both passive (i.e., optical photogrammetry, infrared thermography) and active (i.e., laser, radar) sensors and can measure displacements or collect information on rock mass features (e.g., temperature).

In addition to TLS, two other techniques, i.e., TInSAR and (TIR), were used to collect data on the Mt. Pucci Coastal cliff.

A comprehensive description of the remote survey activities is presented below:

1. a continuous TInSAR monitoring survey with a sampling rate of five minutes was performed from 10 to 12 November 2010, using an IBIS-L (IDS S.p.A.) instrument installed in front of the Mt. Pucci cliff at a distance ranging from 80 m to 150 m (Fig. 4). Hence, 442 SAR (Synthetic Aperture Radar) maps characterized by a range and cross-range resolution of approximately 0.5 m × 0.5 m were collected over the entire monitoring period. Furthermore, a dedicated geo-referencing survey using an artificial corner was used to obtain the 3-D TInSAR displacement map (Fig. 9).

2. IR Thermographic surveys were performed from 10 to 12 November 2010, using the NEC TH7700 camera. Thermal images were collected at different times from two different sensing sites (Fig. 4), thus achieving a wider coverage of the overall cliff and allowing us to investigate the thermal variations of the cliff under different sunlight conditions. Both absolute temperature and thermal changes with time were obtained (Fig. 10).

The TInSAR monitoring allowed us to measure the micro-movements that affected the overall cliff as well as the small blocks. In contrast, the TIR images were intended to obtain information on the thermal features of the rock mass.

Any permanent displacements greater than 1 mm were identified during the monitoring period, whereas certain cyclic movements with a daily variation of 0.5 mm to 1.2 mm were detected at selected localized locations and attributed to thermal variation of the rock mass.

The thermal images allowed us to identify certain positive and negative thermal anomalies (with respect to the mean temperature) at specific locations, which in some cases corresponded to the main fractures (primarily negative anomalies), whereas others in the area were affected by recent collapses (primarily positive anomalies).

7.2 Future monitoring perspectives

Considering the previously introduced evolutionary model for sea cliffs (Fig. 1), monitoring systems should be designed and adapted in terms of the following specific requirements:

1. to investigate or detect cliff slopes at different evolutionary stages (forward prevention), i.e., corresponding to different distributions the landslide hazard;

2. to understand and control the parameters for forecasting the short-term evolution of gravitational instabilities (such as high-velocity landslides) and for the planning of alert systems (real-time prevention).

In this context, the use of geotechnical monitoring (such as extensometers or distantiometers) is particularly well suited for integration with analyses of precursors (Blikra et al., 2005; Bornhold and Thomson, 2012), especially in the "persistent cliff slope stage," when terrestrial interferometric monitoring and laser scanning are more complicated due to the presence of the sea immediately below the cliff. In addition, precursors (such as micro-earthquakes or acoustic emissions) can be analyzed to provide alert systems with information on the impulsive fall events that characterize the persistent or seasonal sea cliff stages (Amitrano et al., 2005; Senfaute et al., 2009).

As the cliff gradually evolves toward a coastal slope (Hutchinson, 1988, 1991), the landslide mechanisms change, and the existence of an emerged beach favors monitoring with remote techniques. At the same time, although the analysis of precursors gradually loses its importance due to the slower sliding mechanisms, strain rate monitoring can indicate evolution toward failure conditions and therefore provide a more responsive strategy for alerts. In this case, innovative ground-based remote sensing techniques (Mazzanti, 2012) such as TLS, TInSAR, TIR represent an opportunity to collect additional data useful for rock cliff characterization but are also promising techniques for designing integrated monitoring systems that aim to collect actions, precursors, and strain effects to provide different levels of monitoring for risk management.

Two different risk management approaches have typically been applied:

1. deterministic approaches that consist of analyzing the recorded data with respect to a "geological model of the natural system" (Angeli et al., 2000; Prestininzi et al., 2012) and providing different levels of sensitivity with respect to possible failure or yielding scenarios;

2. statistical approaches that consist of carrying out a "cloud multi-parametric analysis" (a multisource strategy of investigation) by analyzing all of the collected data in terms of anomaly recurrence (Travelletti et al., 2008; Bigarrè et al., 2011), i.e., deviation from an average behavior, and associating the critical conditions of the natural system with these anomalies (without relating them to an interpretative model).

The first approach was applied in the last several decades for mine monitoring, infrastructure management, tunnel constructions, and landslide monitoring. In the case of mine monitoring, only the precursor events of possible collapses are commonly recorded by integrating acoustic and micro-seismic devices (Phillips et al., 1997; Senfaute et al., 2000; Yang et al., 1998; Lai et al., 2006; Paskaleva et al., 2006), and in the case of infrastructures and tunneling, the warning systems generally manage the actions, precursors, and strain effects separately (Miller et al., 1989; Senfaute et al., 1997; Lenti et al., 2012; Bozzano et al., 2013).

In the case of landslides, the integration of direct and remote sensing techniques for monitoring has been carried out in several cases (Gafet et al., 2010; Bozzano et al., 2012, 2013a,b; Cipriani and Mazzanti, 2012; Blikra, 2012; Loew et al., 2012), but combined alert systems based on multisensor monitoring represent a current challenge.

8 Discussion

The stability conditions of the Mt. Pucci sea cliff were evaluated using a geostructural analysis performed by integrating a direct traditional geomechanical survey and remote

measurements. Two different triggers were considered, which represent the main reliable destabilizing actions for the sea cliff: (i) seismic shaking and (ii) static water filling of the joints. Moreover, a variable weathering condition was taken into account as a predisposing feature for rock block instabilities. Based on the obtained results, both rock topples and rock wedge sliding events may take place (especially in the PSH Fm.) driven by stratification and subvertical joints; the talus at the bottom of the sea cliff slope provides evidence of the frequent occurrence of the fallen blocks. However, the performed susceptibility analyses demonstrated that the actual joint sets do not contribute to sliding block failures. Thus, the pseudo-static critical force that induces topples and sliding failures varies within a range that is sufficiently wide to include the locally expected PGAs, up to 5 % of exceedance in 50 yr. In contrast, the critical height of water filling the joints should reach tens of centimeters to cause topples or sliding failures, which is a severe condition for an intensely jointed rocky slope.

Nevertheless, if the coupled action of weathering and static water fill is taken into account, unstable conditions are generally reached for water levels lower than 47 %, even if 60 % of the weathering is attributed to the joints. This last condition seems more reliable considering that the Mt. Pucci slope is also exposed to sea water atomized by the waves breaking at the bottom of the cliff and is subjected to average seasonal thermal changes of up to 17 °C (derived from the ARPA-Puglia web site, http://www.arpa.puglia.it/web/guest/serviziometeo).

In particular, with reference to the thermal effects on the Mt. Pucci cliff slope, the results achieved in a short-term monitoring experiment via TInSAR and TIR allowed us to improve our understanding of the role of the surveyed joint sets in inducing instabilities in the sea cliff as follows: (i) the thermal images allowed for the identification of certain positive and negative anomalies that correspond to the main joints and to parts of the cliff slope affected by recent collapses; and (ii) the TInSAR monitoring allowed for the measurement of any permanent displacement greater than 1 mm, and selected cyclic movements with a daily base from 0.5 mm to 1.2 mm were detected at certain locations and attributed to the thermal variation of the rock mass.

A relevant feature that should be improved in future expansion of this case study is the analysis of the effects of cyclic and/or dynamic actions such as earthquake shaking, anthropogenic vibrations, and tides. The monitoring of precursor sequences may represent an efficient tool for managing alert conditions because anomalous trends in the records should be related to pre-failure conditions; moreover, the localization of such effects may indicate possible unstable portions of the rock mass.

The most common precursors used for landslide failure prediction are ground displacement/deformation and rainfall (e.g., Fuhrmann et al., 2008; Baum and Godt, 2010; Federico et al., 2012). These two approaches are successfully applied for landslide masses involving both rock and soil characterized by continuum behavior. Hence, these approaches can also be applied for coastal landslides in the “coastal slope” stage (see the evolutionary model in Fig. 1). However, both in the persistent sea cliff and the seasonal sea cliff stages, instability processes occur primarily in rock masses characterized by discontinuous behavior. In this condition, it is more appropriate to examine the joints (e.g., microcracks, joint dilatation) instead of the behavior of the rock mass. Microseismicity techniques, advanced TInSAR processing (Mazzanti and Brunetti, 2010), digital image collation techniques, and TIR may be effective solutions.

Nevertheless, addressing the precursors (e.g., displacements) in discontinuous rock masses is much more complex because they can be characterized by notably low intensity and a short time duration. Indeed, millimeter-scale displacements that take place over a few hours or minutes could correspond to the ultimate stability conditions.

9 Conclusions

The present study demonstrates an integrated approach to the geomechanical characterization of rock cliffs for the analysis of slope stability conditions. To this end, a detailed analysis of the 45 m high Mt. Pucci sea cliff (Gargano promontory, Italy) was performed using different survey techniques and analytical stability methods.

The combination of traditional geomechanical scanlines and remote geostructural investigations using a TLS point cloud allowed us to produce a comprehensive and affordable characterization of the main joint sets, which is the key requirement for performing stability analyses on cliff slopes. Furthermore, this study demonstrates that similar results can be achieved using a traditional survey and a TLS remote survey if advanced data processing is performed. However, the importance of a "mutual support" for attenuating the limitations of both the traditional and remote methods is also clear. Reliable geostructural investigations represent a fundamental feature for the planning of "monitoring systems" that are devoted to assessing and analyzing the stability conditions of rock cliffs for risk mitigation purposes, i.e., by detecting the temporal evolution of specific geomechanical parameters of the rock masses. This application is particularly important for coastal cliffs that are controlled by complex predisposition and triggering factors. More specifically, when applicable, remote sensing techniques are suitable and "safe" solutions for investigating rock cliffs, especially in light of the high density of information they contain.

Data derived from remote sensing techniques may provide more information than that presented in this preliminary monitoring study. For example, information on the rock mass weathering degree and the presence of water in the joints, two of the parameters that control the predisposition to instability of the cliff, can be derived from dedicated TIR surveys.

Monitoring cliff parameters performed by either traditional or remote techniques (the latter including microseismic measurements) may be an effective solution for providing real-time alerts to manage the natural risks associated with rock falls in a coastal area. A primary challenge in this field is to develop multisensory alert systems devoted to collecting the recorded data, analyzing the data in terms of the characteristic parameters, and establishing different thresholds for the hazard level using synthetic "hazard indices" that will notify the relevant risk management authorities.

Acknowledgement. The Authors wish to thank A. Brunetti for his technical support to the monitoring, A. Bretshneider, M. E. Discenza and M. Savina for their contribution to collecting and processing the survey data.

References

Amitrano, D., Grasso, J. R., and Senfaute, G.: Seismic precursory patterns before a cliff collapse and critical point phenomena, Geophys. Res. Lett., 32, L08314, doi:10.1029/2004GL022270, 2005.

Angeli, M. G., Pasuto, A., and Silvano, S.: A critical review of landslide monitoring experiences, Eng. Geol., 55, 133–147, 2000.

Assier-Rzadkiewicz, S., Heinrich, P., Sabatier, P. C., Savoye, B., and Bourillet, J. F.: Numerical modelling of landslide-generated tsunami: the 1979 Nice event, Pure Appl. Geophys., 157, 1707–1727, 2000.

ASTM D5731-08: Standard Test Method for Determination of the Point Load Strength Index of Rock and Application to Rock Strength Classifications, ASTM Ed., 11 pp., 2008.

Barton, N.: Rewiew of a new shear strength criterion for rock joints, Eng. Geol., 7, 287–332, 1973.

Barton, N. and Bandis, V.: Review of predictive capabilities of JRC–JCS model in engineering practice, in: Proceeding of Int. Symposium of Rock Joint, Loen, Norway, Balkema, 603–610, 1990.

Baul, R. L. and Godt, J. W.: Early warning of rainfall-induced shallow landslides and debris flows in the USA, Landslide, 7, 259–272, 2010.

Bigarré, P., Klein, E, Gueniffey, Y., and Verdel, T.: Cloud monitoring: an innovative approach for the prevention of landslide hazards, in: The Second World Landslide Forum Rome, 2011, Abstracts Book WLF2, L16, 475 (free download from the web-site: www.wlf2.org/home/proceedings/WLF2_Abstract_Book_2011.pdf, last access: December 2012), 2011.

Billi, A. and Salvini, F.: Sistemi di fratture associati a faglie in rocce carbonatiche: nuovi dati sull'evoluzione tettonica del Promontorio del Gargano, Boll. Soc. Geol. It., 119, 237–250, 2000.

Blikra, L. H.: The Aknes rockslide, Norway, in: Landslides – Types, Mechanisms and Modeling, edited by: Clague, J. J. and Stead, D., Cambridge University Press, Cambridge, UK, 323–335, 2012.

Blikra, L. H., Longva, O., Harbitz, C., and Løvholt, F.: Quantification of rock avalanche and tsunami hazard in Storfjorden, western Norway, in: Landslide and Avalanches, edited by: Sennest, K., Flaate, K., and Larsen, J. O., Taylor and Francis Group, London, UK, 7–63, 2005.

Bornhold, B. D. and Thomson, R. E.: Tsunami hazard assessment related to slope failures in coastal waters, in: Landslides – Types, Mechanisms and Modeling, edited by: Clague, J. J. and Stead, D., Cambridge University Press, Cambridge, UK, 108–120, 2012.

Bosellini, A. and Morsilli, M.: A lower Cretaceus drawing unconformity on the eastern flank of the Apulia Platform (Gargano Promontory, southern Italy), Cretaceaus Research, 18, 51–61, 1997.

Bosellini, A. and Morsilli, M.: Il Promontorio del Gargano: cenni di geologia ed itinerari geologici, Quaderni del Parco Nazionale del Gargano, 48 pp., 2001.

Bosellini, A., Morsilli, M., and Neri, C.: Long-term event stratigraphy of the Apulia Platform Margin (Upper Jurassic to Eocene, Gargano, southern Italy), J. Sediment. Res., 69, 1241–1252, 1999.

Bozzano, F., Lenti, L., Martino, S., Montagna, A., and Paciello, A.: Earthquake-triggering of landslides in highly jointed rock masses: the 1783 Scilla rock avalanche (Italy), Geomorphology, 129, 294–308, doi:10.1016/j.geomorph.2011.02.025, 2011.

Bozzano, F., Cipriani, I., and Mazzanti, P.: Assessing the efficacy of semi-empirical failure prediction methods for slope affected by human activities, in: Landslides and Engineered Slopes: Protecting Society through Improved Understanding, edited by: Eberhardt, E., Froese, C., Turner, K., and Leroueil, S., Taylor & Francis Group, London, 1465–1471, 2012.

Bozzano, F., Mazzanti, P., and Prestininzi, A.: Supporting tunneling excavation of an unstable slope by long term displacement monitoring, Seventh International Conference on Case Histories in Geotechnical Engineering (Chicago, USA, 29 April–4 May 2013), in press, 2013a.

Bozzano, F, Cipriani, I., Martino, S., Mazzanti, P., and Prestininzi, A.: Forecasting methods for landslides interacting with infrastructures, in: Landslide Science and Practice, Social and Economic Impact and Policies, Vol. 7, edited by: Margottini, C., Canuti, P., and Sassa, K., in press, 2013b.

Cipriani, I. and Mazzanti, P.: Analisi del comportamento deformativi pre-rottura di frane superficiali tramite monitoraggio con Interferometria SAR Terrestre, Eng. Hydro. Env. Geology, 14, 66–67, doi:10.1474/EHEGeology.2012-14.B.79, 2012.

De Vallejo, L. G.: Geoingegneria, Pearson Education Italia S.r.l., Milano, 2005.

DISS Working Group: Database of Individual Seismogenic Sources (DISS), Version 3.1.1: a compilation of potential sources for earthquakes larger than M 5.5 in Italy and surrounding areas, available at: http://diss.rm.ingv.it/diss/ (last access: December 2012), ©INGV 2010 – Istituto Nazionale di Geofisica e Vulcanologia – All rights reserved, 2010.

Duncan, C. W. and Christopher, W. M.: Rock Slope Engineering: Civil and Mining, Taylor & Francis, pp. 431, 2004.

Duperret, A., Genter, A., Martinez, A., and Mortimore, R. N.: Coastal chalk cliff instability in NW France: the role of lithology, fracture pattern and rainfall, in: Coastal Chalk Cliff Instability, edited by: Mortimore, R. N. and Duperret, A., Geological Society, London, Eng. Geol. Sp., 20, 33–55, 2004.

Duperret, A., Genter, A., Martinez, A., Mortimore, R. N., Delacourt, B., and Pomerai, M. R.: Coastal rock cliff erosion by collapse at Puys, France: the role of impervious seams within chalk of NW Europe, J. Coastal Res., 18, 52–61, 2002.

Emery, K. O. and Kuhn, G. G.: Sea cliffs: their processes, pro-files, and classification, Geological Society America Bulletin, 93, 644–654, 1982.

Federico, A., Popescu, M., Elia, G., Fidelibus, C., Interno, G., and Murianni, A.: Prediction of time to slope failure: a general framework, Environ. Earth Sci., 66, 245–256, 2012.

Fine, I. V., Rabinovich, A. B., Bornhold, B. D., Thomson, R. E., and Kulikov, E. A.: The Grand Banks landslide-generated tsunami of 18 November 1929, preliminary analysis and numerical modeling, Mar. Geol., 215, 45–57, 2005.

Fortunato, C., Martino, S., Prestininzi, A., and Romeo, R. W.: New release of the Italian catalogue of earthquake-induced ground failures (CEDIT), Italian Journal of Engineering and Geology and Environment, 2, 63–74, 2012.

Fuhrmann, C. M., Konrad, C. E., and Band, L. E.: Climatological perspectives on the rainfall characteristics associated with landslides in western North Carolina, Phys. Geogr., 29, 289–305, 2008.

Gaffet, S., Guglielmi, Y., Cappa, F., Pambrun, C., Monfret, T., and Amitrano, D.: Use of the simultaneous seismic, GPS and meteorological monitoring for the characterization of a large

unstable mountain slope in the southern French Alps, Geophys. J. Int., 182, 1395–1410, 2010.

Goodman, R. E. and Bray, J. W.: Toppling of rock slopes, in: Rock Engineering for Foundations and Slopes, Proceedings of a Specialty Conference, Vol. 2, Am. Soc. Civ. Eng. New York, 201–233, 1976.

Hampton, M. A., Griggs, G. B., Edil, T. B., Guy, D. E., Kelley, J. T., Komar, P. D., Mickelson, D. M., and Shipman, H. M.: Processes that govern the formation and evolution of coastal cliffs, in: Formation, Evolution, and Stability of Coastal Cliffs – Status and Trends, edited by: Hampton, M. A. and Griggs, G. B., USGS – Professional Paper 1693, 1–4, 7–38, 2004.

Hampton, M. A., Griggs, G. B., Edil, T. B., Guy, D. E., Kelley, J. T., Komar, P. D., Mickelson, D. M., and Shipman, H. M.: Formation, evolution, and stability of coastal cliffs – status and trends: introduction, in: Formation, Evolution, and Stability of Coastal Cliffs – Status and Trends, edited by: Hampton, M. A. and Griggs, G. B., USGS – Professional Paper 1693, 1–4, 2004.

Hatheway, H. W.: The complete ISRM suggested methods for rock characterization, testing and monitoring, 1974–2006, Environ. Eng. Geosci., 15, 47–48, doi:10.2113/gseegeosci.15.1.47., 2009.

Heezen, B. C. and Ewing, M.: Turbidity currents and submarine slumps, and the 1929 Grand Banks Earthquake, Am. J. Sci., 250, 849–873, 1952.

INGV: Mappa di pericolosità sismica del territorio nazionale, available at: http://esse1.mi.ingv.it/ (last access: December 2012), 2006.

ISPRA: Atlante Italiano delle Coste, available at: http://www.isprambiente.gov.it/it/servizi-per-lambiente/stato-delle-coste/atlante-delle-coste (last access: December 2012), 2012.

ISRM: Suggested Methods for Determining Water Content, Porosity, Density, Absorption and Related Properties and Swelling and Slake-Durability Index Properties, 1977.

ISRM: Suggested methods for the quantitative description of discontinuities in rock masses, International Journal of Rock Mechanics Mining Sciences & Geomechanics, available at: http://www.isrm.net/gca/?id=177 (last access: December 2012), 1978.

ISRM: Suggested methods for determining point load strength, international society for rock mechanics commission on testing methods, Int. J. Rock. Mech.Min. Sci., and Geomechanical Abstr., 22, 51–60, 1985.

ISRM: The Complete ISRM Suggested Methods for Rock Characterization, Testing and Monitoring: 1974–2006, edited by: Ulusay, R. and Hudson, J. A., Suggested Methods Prepared by

the Commission on Testing Methods, International Society for Rock Mechanics, Compilation Arranged by the ISRM Turkish National Group, Ankara, Turkey, 628 pp., 2007.

Jaboyedoff, M., Metzger, R., Oppikofer, T., Couture, R., Derron, M. H., Locat, J., and Turmel, D.: New insight techniques to analyze rock-slope relief using DEM and 3-D-imaging cloud points: COLTOP-3-D software, in: Rock Mechanics: Meeting Society's Challenges and Demands (Vol. 1), edited by: Eberhardt, E., Stead, D., and Morrison, T., Taylor & Francis, 61–68, doi:10.1201/NOE0415444019-c8, 2007.

L'Heureux, J. S., Eilertsen, R. S., Glimsdal, S., Issler, D., Solberg, I. L., and Harbitz, C. B.: The 1978 quick clay landslide at Rissa, mid Norway: subaqueous morphology and tsunami simulations, in: Proceedings of the 5th International Symposium on Submarine Mass Movements and Their Consequences, edited by: Yamada, Y., Kawamura, K., and Ikehara, K., Springer Science + Business Media, Kyoto, Japan, 2011.

Lai, X. P., Cai, M. F., and Xie, M. W.: In situ monitoring and analysis of rock mass behavior prior to collapse of the main transport roadway in Linglong Gold Mine, China, International Journal of Rock Mechanics & Mining Sciences, 43, 640–646, 2006.

Lee, E. M., Hall, J. W., and Meadowcroft, I. C.: Coastal cliff recession: the use of probabilistic prediction methods, Geomorphology, 40, 253–269, 2001.

Lee, E. M., Meadowcroft, I. C., Hall, J. W., and Walkden, M.: Coastal landslide activity: a probabilistic simulation model, B. Eng. Geol. Environ., 61, 347–355, 2002.

Lenti, L., Martino, S., Paciello, A., Prestininzi, A., and Rivellino, S.: Microseismicity within a karstified rock mass due to cracks and collapses triggered by earthquakes and gravitational deformations, Nat. Hazards, 64, 359–379, 2012.

Lim, M., Rosser, N. J., Allison, R. J., and Petley, D. N.: Erosional processes in the hard rock coastal cliffs at Staithes, North Yorkshire, Geomorphology, 114, 12–21, 2010.

Loew, S., Gischig, V., Willenberg, H., Alpiger, A., and Moore, J.: Randa: kinematics and driving mechanisms of a large complex rockslide, in: Landslides – Types, Mechanisms and Modeling, edited by: Clague, J. J. and Stead, D., Cambridge University Press, Cambridge, UK, 297–309, 2012.

Markland, J. T.: A Useful Technique for Estimating the Stability of Rock Slopes When the Rigid Wedge Slide Type of Failure Is Expected: Imperial College Rock Mechanics Research Reprints, n. 19, 1972.

Marques, F. M. S. F.: Magnitude-frequency of sea cliff instabilities, Nat. Hazards Earth Syst. Sci., 8, 1161–1171, doi:10.5194/nhess-8-1161-2008, 2008.

Marques, F., Matildes, R., and Redweik, P.: Statistically based sea cliff instability hazard assessment of Burgau-Lagos coastal section (Algarve, Portugal), J. Coastal Res., Special Issue, 64, 927–931, 2011.

Mazzanti, P.: Displacement monitoring by Terrestrial SAR Interferometry for geotechnical purposes, Geotechnical News, June 2011, 25–28, 2011.

Mazzanti, P.: Remote monitoring of deformation, an overview of the seven methods described in previous GINs, Geotechnical News, December 2012, 24–29, 2012.

Mazzanti, P. and Bozzano, F.: Revisiting the 6 February 1783 Scilla (Calabria, Italy) landslide and tsunami by numerical simulation, Mar. Geophys. Res., 32, 273–286. 2011.

Mazzanti, P. and Brunetti, A.: Assessing rockfall susceptibility by Terrestrial SAR Interferometry, in: Proceedings of the Mountain Risks International Conference, Firenze, Italy, 24–26 November 2010, edited by: Malet, J. P., Glade, T., and Casagli, N., 109–114, 2010.

Miller, A., Richards, J. A., McCann, D. M., Browitt, C. W. A., and Jackson, P. D.: Microseismic techniques for monitoring incipient hazardous collapse conditions above abandoned limestone mines, Q. J. Eng. Geol., 22, 1–18, 1989.

Mortimore, R. N., Lawrence, J., Pope, D., Duperret, A., and Genter, A.: Coastal cliff geohazards in weak rock: the UK chalk cliffs of Sussex, in: Coastal Chalk Cliff Instability, edited by: Mortimore, R. N. and Duperret, A., Geological Society, London, Eng. Geol. Sp., 20, 3–31, 2004.

Papadopoulos, G. A. and Kortekaas, S.: Characteristics of landslide generated tsunamis from observational data, in: Submarine Mass Movements and their Consequence, Advances in Natural and Technological Hazards Research, 19, edited by: Locat, J. and Mienert, J., Kluwer Academic Publishers, 267–374, 2003.

Paskaleva, I., Aronov, A. G., Seroglazov, R. R., and Aronova, T. I.: Characteristic features of induced seismic processes in mining regions exemplified by the potassium salt deposits in Belarus and Bulgaria, Acta Geod. Geoph. Hung., 41, 293–303, 2006.

Phillips, W. S., Pearson, D. C., Edwards, C. L., and Stump, B. W.: Microseismicity induced by a controlled, mine collapse at white pine, Michigan, International Journal of Rock Mechanics & Mining Sciences, 34, paper 246, 1997.

Polemio, M., Di Cagno, M., and Virga, R.: Le acque sotterranee del Gargano: risorse idriche integrative e di emergenza, Acque sotterranee, 68, 41–58, 2000.

Prestininzi, A., Bianchi-Fasani, G., Bozzano, F., Esposito, C., Martino, S., Mazzanti, P., and Scarascia-Mugnozza, G.: From the refinement of geological models to risk management:

the role of landslide monitoring, in: Landslides and Engineered Slopes: Protecting Society through Improved Understanding, edited by: Eberhardt, E., Froese, C., Turner, K., and Leroueil, S., 2012 Taylor & Francis Group, London, 2012.

Senfaute, G., Chambon, C., Bigarre, P., Guise, Y., and Josien, J. P.: Spatial distribution of mining tremors and the relationship to rockburst hazard, Pure Appl. Geophys., 150, 3–4, 1997.

Senfaute, G., Abdul Wahed, M., Lenhard, F., and Morel, J.: Technique d'écoute microsismique appliquée au risqué d'effondrement dans les mines du bassin ferrifère lorrain, Revue Française de Géotechnique, 92, 57–62, 2000.

Senfaute, G., Duperret, A., and Lawrence, J. A.: Micro-seismic precursory cracks prior to rockfall on coastal chalk cliffs: a case study at Mesnil-Val, Normandie, NW France, Nat. Hazards Earth Syst. Sci., 9, 1625–1641, doi:10.5194/nhess-9-1625-2009, 2009.

Tappin, D. R., Watts, P., McMurtry, G. M., Lafoy, Y., and Matsumoto, T.: The Sissano, Papua New Guinea tsunami of July 1998 – offshore evidence on the source mechanism, Mar. Geol., 175, 1–23, 2001.

Tinti, S., Maramai, A., and Graziani, L.: The new catalogue of Italian tsunamis, Nat. Hazards, 33, 439–465, 2004.

Travelletti, J., Oppikofer, T., Delacourt, C., Malet, J. P., and Jaboyedoff, M.: The International Archives of the Photogrammetry, Remote Sensing and Spatial Information Sciences, Vol. XXXVII, Part B5, Beijing, 2008.

Violante, C.: Geohazard in Rocky Coastal Areas, Geological Society, London, Special Publications, 322, 2009.

Yang, X., Stump, B. W., and Phillips, W. S.: Source mechanism of an explosively induced mine collapse, B. Seismol. Soc. Am., 88, 843–854, 1998.

Table 1. Joint parameters from the direct geomechanical scanlines.

Lithology	Joint set	Dip Direction azimuth	Dip (°)	Spacing (cm)	Jv (joint m^{-3})	Ib (cm)
PSH	J1(strata)	24	11	59		
PSH	J2	247	65	40	8	69
PSH	J3	270	87	36		
PSH	J4	301	87	62		
PSH	J5	360	81	53		
SC	J1(strata)	23	16	24	12.5	25
SC	J2	258	68	21		

Table 2. Physical and mechanical properties of the PSH and SC intact rock from the laboratory tests and the point load tests.

Lithology	γ_s (kN m^{-3})	γ_n (kN m^{-3})	$I_{s(50)}$ (MPa)	q_c (20–25 % I_s 50) (MPa)
PSH	26.80	23.44	3.11	62.11–77.63
SC	26.86	23.23	3.18	63.51–79.38

Table 3. Joint parameters from the remote measurements.

Lithology	Joint set	Dip Direction azimuth	Dip (°)	Spacing (cm)	Jv (joint m^{-3})	Ib (cm)
PSH	J1(strata)	20	15	64		
PSH	J2	253	75	39	3.2	54
PSH	J3	300	82	59		
PSH	J4	350	87	54		
SC	J1(strata)	28	10	21	9.7	44
SC	J2	120	82	67		

Table 4. Geomechanical properties attributed to the recognized joint sets: JRC–Joint Roughness Coefficient, JCS–Joint Compressive Strength (Barton and Bandis, 1973, 1990), σ_n – normal stress acting on the joints, φ_b – intact rock fiction angle, φ_p – joint friction angle, φ_p – residual joint friction angle, r/R – weathering joint ratio, φ_p – weathered friction angle (De Vallejo, 2005).

Lithology	Joint set	Dip Direction azimuth	Dip (°)	Spacing (cm)	JCS (MPa)	JRC	σ_n (kPa)	ϕ_b (°)	ϕ_p (°)	r/R	ϕ_r (°)	ϕ_{wth} (°)
PSH	J1(strata)	21	15	64	64	10	129	34	31	0.2	18	15
PSH	J2	300	88	59	46	12	129	34	29	0.4	22	17
PSH	J3	358	90	54	45	17	129	34	26	0.6	26	18
PSH	J4	269	87	34	44	14	129	34	27	0.8	30	23
PSH	J5	253	70	39	44	18	129	34	26	1	34	26
SC	J1(strata)	25	10	21	40	14	128	31	24	nd	nd	nd
SC	J2	300	80	67	42	12	128	31	25	nd	nd	nd

Table 5. Joint combinations and related rock block geometries compatible with topples at the Mt. Pucci cliff slope (see the manuscript for the used symbols).

slope face (dip dir/dip)	basal joint (dip dir/dip)	lateral joint_1 (dip dir/dip)	lateral joint_2 (dip dir/dip)	spacing_1 (m)	spacing_2 (m)	H (m)	b (m)	ψ (°)	ϕ (°)
355/80	21/15	300/88	358/90	0.59	0.55	0.64	0.55	15	31
355/80	21/15	300/88	253/70	0.59	0.39	0.64	0.48	15	31
355/80	21/15	300/88	269/87	0.59	0.34	0.64	0.5	15	31
355/80	21/15	358/90	269/87	0.54	0.34	0.64	0.64	15	31
355/80	21/15	358/90	253/70	0.54	0.39	0.64	0.64	15	31
355/80	21/15	269/87	253/70	0.34	0.39	0.65	0.38	15	31

Table 6. Stability analysis of rock wedges at Mt. Pucci: $Z\mathrm{w}_{cr}$ – critical height of the static water filling the joints; k_y – pseudo-static critical acceleration; SF_{475} – safety factor computed for a pseudo-static seismic action with a return time of 475 yr; $\mathrm{SF2}_{475}$ – safety factor computed for a pseudo-static seismic action with a return time of 2475 yr; $\mathrm{SF}_{r/R}$ – safety factor for weathered joint conditions (r/R is the weathering joint ratio; De Vallejo, 2005).

slope face (dip dir/dip)	joint sets	$Z\mathrm{w}_{cr}$ (m)	k_y (g)	SF_{475} yr (k_x = 0.169 g)	SF_{2475} yr (k_x = 0.316 g)	$\mathrm{SF}_{r/R}$ 0.2	0.4	0.6	0.8	1
300/60	J1–J4	0.38	0.07	< 1	< 1	< 1	1.2	1.5	1.7	2.6
300/60	J1–J5	0.55	0.44	1.7	1.2	1.1	1.5	1.9	2.3	3.3
320/75	J1–J2	0.2	< 0.05	< 1	< 1	< 1	< 1	1.3	1.5	2.2
320/75	J1–J4	0.48	0.46	1.8	1.3	< 1	1.2	1.5	1.8	2.6
320/75	J1–J5	0.65	0.37	1.6	1.1	1.2	1.5	1.9	2.3	3.3
345/70	J1–J2	0.4	< 0.05	< 1	< 1	< 1	1.0	1.3	1.5	2.2
345/70	J1–J4	0.48	0.48	1.9	1.4	< 1	1.2	1.5	1.8	2.6
345/70	J1–J5	0.65	0.66	2.7	1.9	1.2	1.5	1.9	2.3	3.3
355/80	J1–J2	0.5	< 0.05	< 1	< 1	< 1	1.0	1.3	1.5	2.2
355/80	J1–J4	0.58	0.50	2	1.5	< 1	1.2	1.5	1.8	2.6
355/80	J1–J5	0.65	0.78	3.1	2.1	1.1	1.5	1.9	2.3	3.3
330/70	J1–J2	0.3	< 0.05	< 1	< 1	< 1	1.0	1.2	1.5	2.2
330/70	J1–J4	0.48	0.45	1.7	1.2	< 1	1.2	1.5	1.8	2.6
330/70	J1–J5	0.55	0.36	1.5	1.1	1.2	1.5	1.9	2.3	3.3

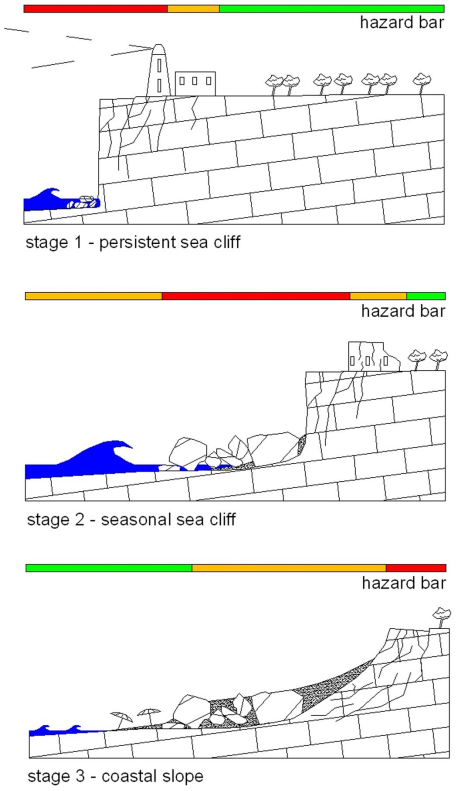

Fig. 1. Conceptual model showing the evolution from a sea cliff to a cliff slope and the related hazard levels (colored scale: red – severe hazard, orange – low hazard, green – very low hazard).

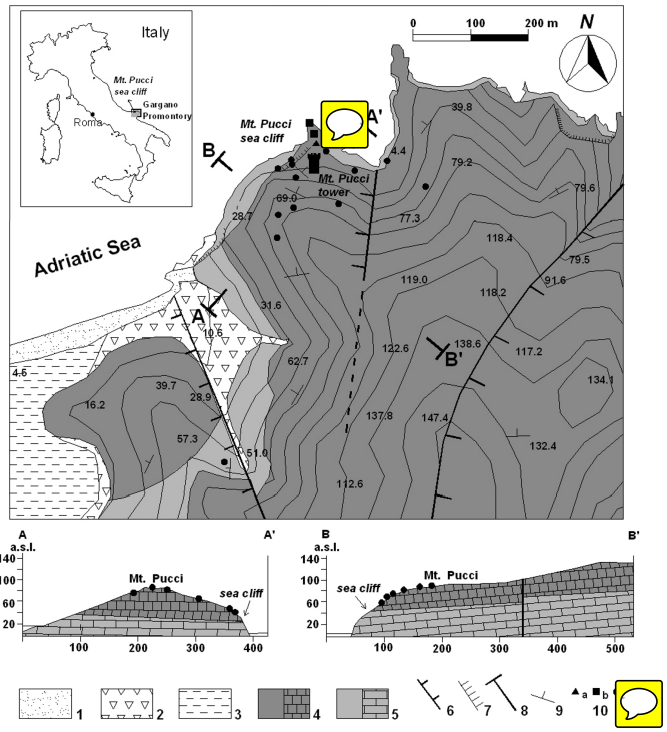

Fig. 2. Geological sketch of the Mt. Pucci coastal area: (1) coastal deposits; (2) slope debris; (3) alluvia; (4) calcarenites of the Peschici Formation (PSH), Eocene; (5) marly limestones of the Scaglia Formation (SC), lower–middle Cretaceous; (6) certain fault; (7) cliff scarp; (8) trace of geological section; (9) attitude of beds; (10) measurement points: a – remote sensing, b – laser scanner, c – geomechanical scanlines.

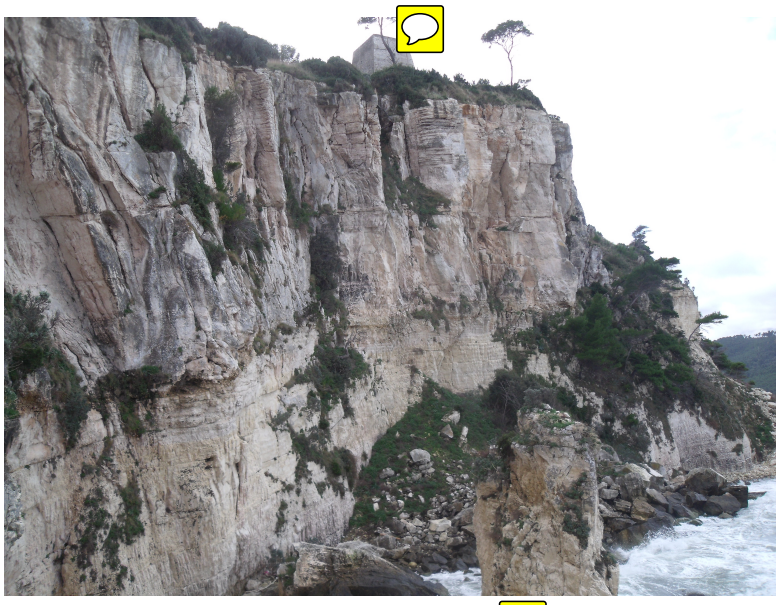

Fig. 3. Photo view of the Mt. Pucci cliff slope from the remote sensing point shown in Fig. 2.

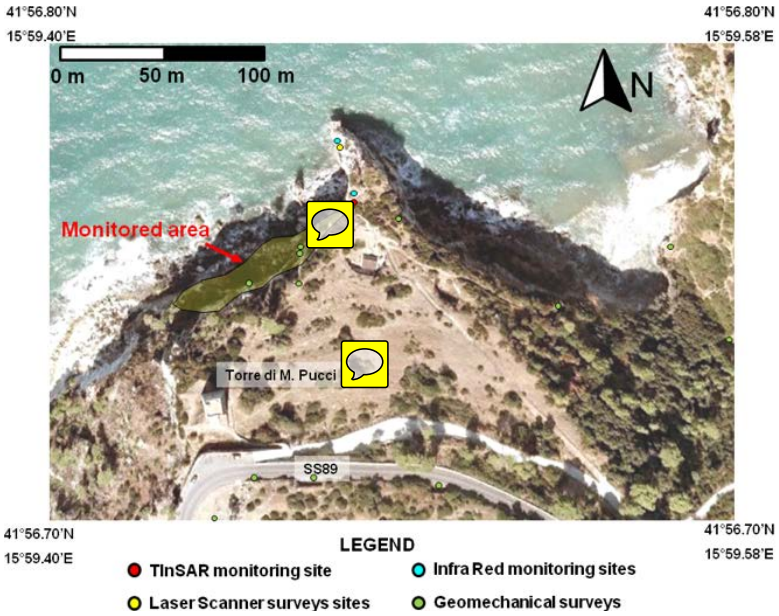

Fig. 4. Aerial photo of the Mt. Pucci area showing the investigated sector (Mt. Pucci Cliff); the locations of the TInSAR, TLS, and TIR remote surveys; and the geomechanical stations.

Fig. 5. TLS point cloud of the Mt. Pucci cliff: left: the standard point cloud; right: the point cloud colored by the optical photos.

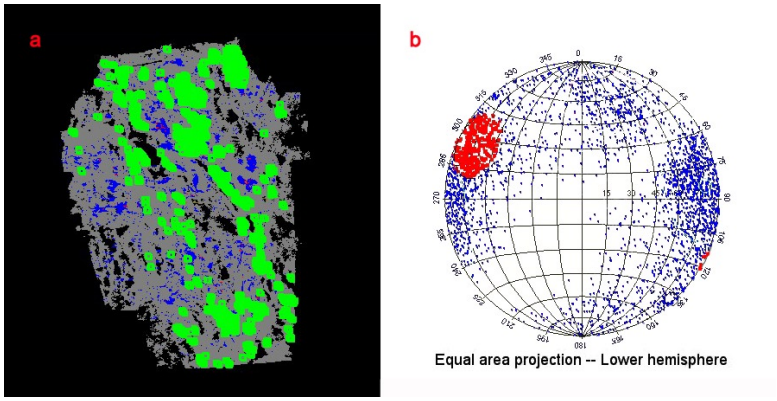

Fig. 6. Sketch showing the results of the automatic detection of the main joint sets from a Laser Scanner georeferenced points cloud; **(a)** points cloud of aportion of the cliff (grey colour) with the automatic identification of planes (blue colour) and selection of some planes of the same joint set (green dots); **(b)** stereoplot showing the poles of the planes automatically detected (blue dots) on the points could and poles selected on the side image (red dots).

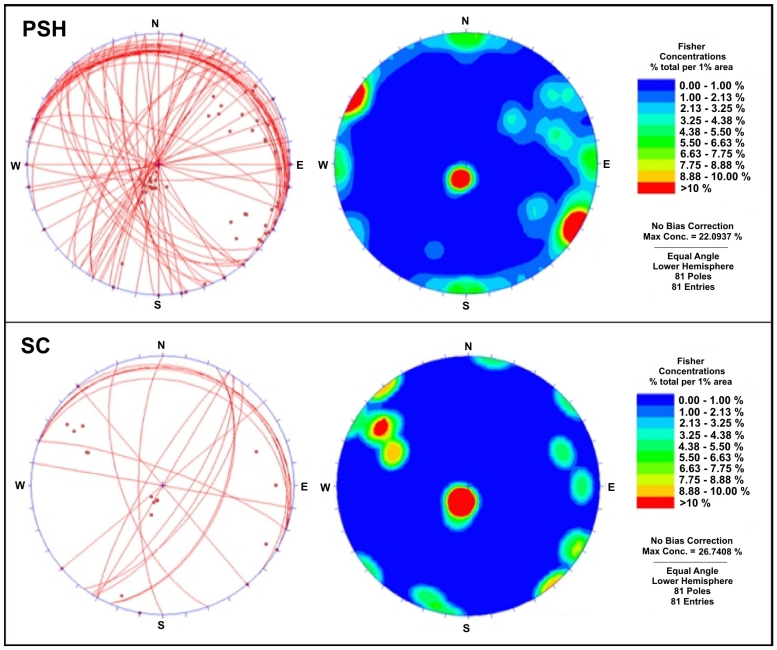

Fig. 7. Great circles and stereo-plots for PSH Fm. and SC Fm. referenced to the geomechanical measurements from direct and remote surveys.

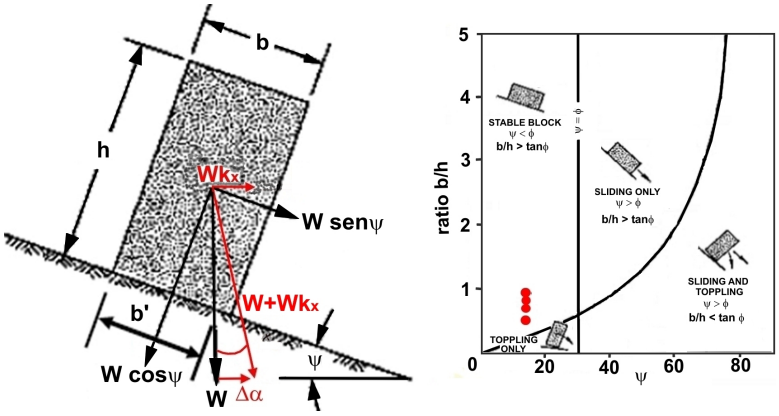

Fig. 8. Stability chart for rock topples (modified from Goodman and Bray, 1976); the red circles correspond to the rock blocks of the Mt. Pucci cliff slope.

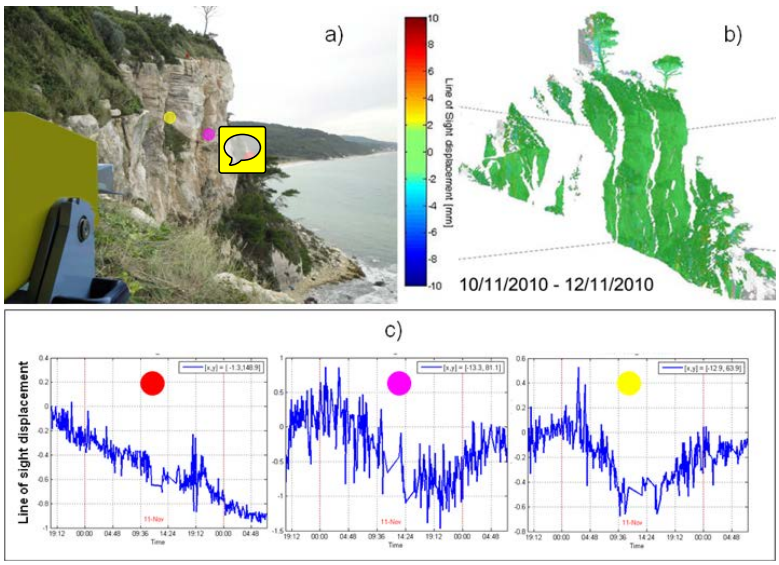

Fig. 9. (a) Picture showing the Terrestrial SAR Interferometer installed in front of the Mt. Pucci cliff slope; **(b)** TInSAR map of displacement projected on the 3-D TLS point cloud; **(c)** time series of displacements of three points located on the cliff (colored circles identify the corresponding point location on the cliff slope).

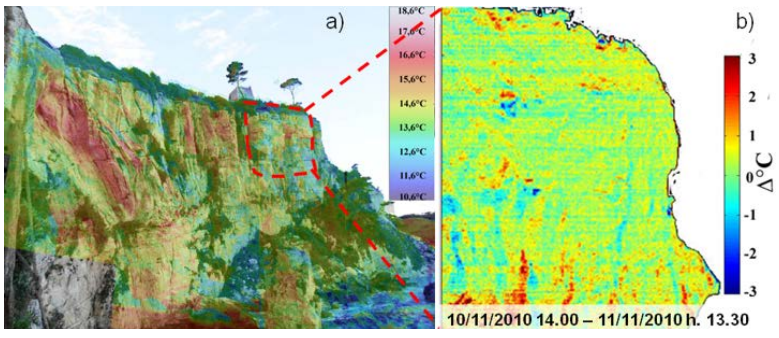

Fig. 10. (a) Thermal static map of the overall Mt. Pucci cliff slope; **(b)** differential thermal map of a localized sector of the Mt. Pucci cliff slope.